PROCEEDINGS OF SCIENCE

Measurement of the cosmic ray proton spectrum around the knee region with LHAASO

You Zhiyong,[a,c,*] **Zhang Shoushan,**[a,c] **Yin Liqiao,**[a,c] **Ma Lingling,**[a,c] **Cao Zhen**[a,b,c] **and Wang Yudong**[a,c] **for the LHAASO collaboration**

[a] *The Institute of High Energy Physics of the Chinese Academy of Sciences, YuQuan Road.19B, shijingshan district, Beijing, China*

[b] *University of Chinese Academy of Sciences, Department, YuQuan Road.19A, shijingshan district, Beijing, China*

[c] *TIANFU Cosmic Ray Research Center, Chengdu, Sichuan, China*

E-mail: youzhiyong@ihep.ac.cn, yinlq@ihep.ac.cn, wangyd89@ihep.ac.cn

One of the main scientific aims of LHAASO is to measure the energy spectra of cosmic rays for individual mass compositions. LHAASO is made up of three detector arrays, which are WFCTA, KM2A, and WCDA. The three detector arrays can achieve hybrid observation, so several extensive air shower observables that are sensitive to mass compositions can be measured simultaneously. ROOT-TMVA package is used to combine these component-sensitive parameters for selecting proton events. The selected proton events have a purity of over 90%. In this paper, we have selected simulated events with shower cores located in the KM2A array to investigate the feasibility of the analysis method for studying the proton energy spectrum. We have also studied the associated systematic uncertainties, including those introduced by the composition models, proton selection, energy reconstruction method, and hadronic interaction models.

38th International Cosmic Ray Conference (ICRC2023)
26 July - 3 August 2023
Nagoya, Japan

ICRC2023
38th International Cosmic Ray Conference
The Astroparticle Physics Conference

*Speaker

PoS(ICRC2023)423

1. Introduction

Measurement of individual cosmic ray spectra especially near the "knee" region is important to investigate cosmic ray acceleration and propagation mechanisms. However, there is no definite conclusion on the single component cosmic ray spectrum around the "knee" region on the observational results. This is because of the difficulties of separating individual cosmic ray composition with high purity and lack of the absolute energy calibration for ground-based experiments.

Large High Altitude Air Shower Observatory (LHAASO) is situated on Mount Haizi, Sichuan Province, China, at an altitude of 4,410 meters. One of the main scientific goals of LHAASO is to measure the single component, or mass groups, energy spectrum through the "knee" [1]. LHAASO contains three kinds of sub-detector arrays, namely the square kilometer array (KM2A), the water Cherenkov detector array (WCDA), and the wide field-of-view Cherenkov telescope array (WFCTA). Different arrays in LHAASO simultaneously measure various secondary particle parameters in an extensive air shower (EAS). These parameters characterize EASs induced by various primary particles. Combined analysis of these parameters makes the LHAASO enable to identify the composition of cosmic rays event by event with high purity.

After the description of the data used in Section 2, the analysis approach is outlined in Section 3. The main topics in Section 3 are energy reconstruction and joint analysis of multiple component discrimination variables to select high-purity protons. In Section 4, the uncertainties from composition models, the proton selection, the energy reconstruction method, and interaction models are discussed. Section 5 summarizes the main conclusions of this work.

2. Simulation and data selection

The EAS simulation is made via CORSIKA(v7.7410)[2]. The EGS4 model is used for electromagnetic interactions, while the QGSJETII-04[3] and FLUKA[4] models are used for high(>80GeV) and low(<80GeV) energy hadronic interactions, respectively. Five groups of primary particles are generated in the simulation: protons, helium nuclei, CNO group, MgAlSi group, and iron nuclei. The zenith and azimuth angles range from 20° to 40° and 5° to 185°, respectively. The core position range is 300 m × 300 m, with the origin at the center of the telescope array. The energy range is from 10 TeV to 10 PeV, generated with an energy spectral index of -1.

The observation period used for this work was taken from November 2020 to March 2021. The data include information from KM2A half-array and WFCTA. Atmospheric Cherenkov light attenuates during its propagation, so to reduce the impact of atmospheric extinction on WFCTA observations, it is necessary to select the atmospheric quality. An infrared cloud monitor, providing the infrared brightness temperature (T_b) for the entire sky every 10 minutes, is installed at the LHAASO site to monitor the weather. A lower value of T_b indicates less water vapor content and less cloud cover. In this work, $T_b < -65$°C is chose. The photo-detector used in the camera of WFCTA is silicon photomultipliers (SiPM). The gain of the SiPM is affected by the intensity of the background light. Moonlight is the primary source of background light, so it is necessary to select events according to the state of the moon to ensure accurate observations. In this work, The space angle between the telescope and moon is larger than 30°, and the moon phase with less than 60% illumination is applied.

To ensure the quality of event reconstruction. The following event selections are applied: (1) the distance between the core reconstructed by KM2A and the edge of KM2A half-array is larger than 50 m. The core region and detector setup are shown in Fig.1; (2) number of triggered EDs is more than 20; (3) number of electromagnetic particles recorded by EDs within a circle with a radius of 100 m is greater than that within a ring from 40 m to 100 m by a factor of 2; (4) the perpendicular distance from the telescope to the shower axis (R_p) is limited between 90 m and 200 m; (5) the angular distance between the centroid of the Cherenkov image and the edge of the camera is greater than 3°; (6) more than 10 triggered pixels in the Cherenkov image. The measured data is reconstructed using the same reconstruction algorithm applied to the simulations. After the event selection, the angular and shower core position resolution is less than 0.3° and 3 m above 200 TeV, respectively. The observation time is about 569 hours. The data set has a total of 4 $\times 10^6$ showers. The effective aperture is about 9,934 m^2Sr for proton events.

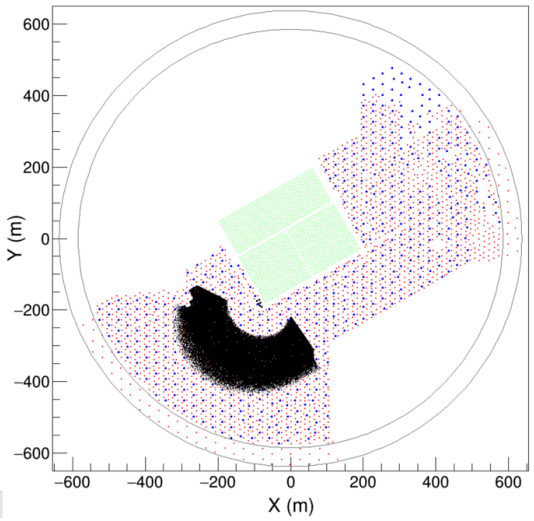

Figure 1: The red dots represent EDs. The blue dots represent MDs. The green square represents WCDA. The black region represents the shower core position range of the selected events.

3. Description of the analysis

Information from telescopes and ground-based arrays about these events is related to the primary energy of the particles and can therefore be used to reconstruct energy. By using multivariate analysis to select components, high-purity protons can be obtained. The process involves first reconstructing the event energy, followed by selecting individual events to obtain selected protons, and then obtaining the energy spectrum.

3.1 Energy reconstruction

Energy reconstruction by ED and MD: The altitude of LHAASO is near the maximum of EASs, so the fluctuation of measurement of ED and MD for electromagnetic particles and muons is minimal. Combining ED and MD to reconstruct energy can not only effectively reduce the component dependence in primary energy, but also improve energy resolution[5]. The KM2A half-array was used in this work, so the number of electromagnetic particles (N_e) and number of muons (N_μ) within 40-200 m from the shower axis cannot represent all the electromagnetic particles and muons. We calculate N_e and N_μ using the same approach as [6]. Combining N_e and N_μ, the energy can be reconstructed as:

$$E_{rec} = a \times (N_e + 52 \times N_\mu) \quad (1)$$

Where the parameter $a = 2.21\ GeV$ is obtained by fitting the relationship between primary energy and $N_e + 52 \times N_\mu$ for proton events. For proton events, the energy bias is below 5% and energy resolution improves as energy increases and is better than 20% above 300 TeV (shown in Fig.2).

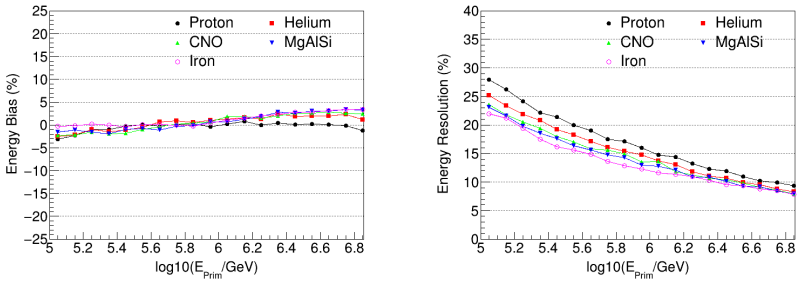

Figure 2: Left and right show the energy bias and energy resolution in different energy regions for individual components. Energy is reconstructed by combining N_e and N_μ.

Energy reconstruction by WFCTA and MD: Since most Cherenkov photons are produced by electromagnetic particles, the intensity of photons measured by the telescope can be representative of the electromagnetic component in the EASs. The combination of total Cherenkov photons detected by telescope (N_{Size}) and N_μ can also be used to reconstruct energy. Details of the energy reconstruction method can be found in [6]. For proton events, the energy bias is below 5% and energy resolution is better than 18% (shown in Fig.3).

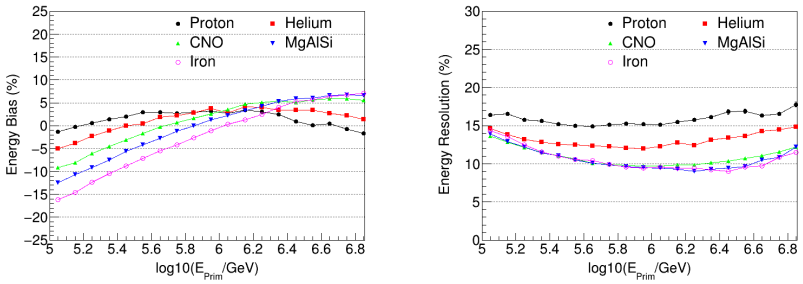

Figure 3: Left and right show the energy bias and energy resolution in different energy regions for individual components. Energy is reconstructed by combining N_{Size} and N_μ.

3.2 Proton selection

Proton-induced EAS has a deeper atmospheric depth of shower maximum than heavier particles. The angular distance from the Cherenkov image centroid to the shower direction (D_{dist}) is used to construct component-sensitive parameters in this work. At the same energy, the secondary particles in showers induced by heavier primaries are spread further away from the core region than proton events. Besides, there are more muons and fewer electromagnetic particles in heavier showers. Thus the number of electromagnetic particles within 20 m from the core region (N_e^{20}) and the ratio of muon and electromagnetic particles (ρ_μ/ρ_e) can be used to construct component sensitive parameters. Here we choose two sets of MD and ED ring bands to take into account the component identification ability of different energy regions. They are $\rho_\mu^{40-200}/\rho_e^{40-100}$ and $\rho_\mu^{100-300}/\rho_e^{100-200}$. D_{dist} and N_e^{20} are related to both components and energy. D_{dist} and N_e^{20} can

be corrected using the reconstructed energy to eliminate their energy dependence and obtain the component identification parameters P_{Dist} and $P_{N_{e20}}$. The distributions of P_{Dist} and $P_{N_{e20}}$ are shown in Fig.4(a). The Blue and red distributions represent protons and other heavier components, respectively. Note that the values of the parameters are shifted to ensure that the mean value of the proton distribution is around 0. The parameters P_{mue} and P_{mue2} constructed from $\rho_{\mu}^{40-200}/\rho_{e}^{40-100}$ and $\rho_{\mu}^{100-300}/\rho_{e}^{100-200}$ are also shown in Fig.4(a).

ROOT-TMVA is used to combine the four parameters to select proton events. Events are randomly and equally divided into two parts for training and testing. Here Boosted Decision Trees with Gradient boosting (BDTG) is chosen in TMVA training. To avoid overtraining, some of the configuration options in TMVA are set: (1) number of trees in the forest is 200; (2) number of grid points used in finding optimal cut in node splitting is 20; (3) maximum depth of the decision tree is 2. The training result is shown in Fig.4(b). After TMVA training, the final discriminating parameters S_{TMVA} can be obtained. The relationship between the S_{TMVA} of protons (black filled circles) and other components (red open squares) and energy is shown in Fig.5(a). The error bar is the root mean square (RMS) of the two distributions. The selection condition, $S_{TMVA} > -0.0315 \times \lg^2 E + 0.325 \times \lg E + 0.08$, is used to select proton events. After the cut described above, the selection efficiency and purity of the proton are approximately 23% and 90%, respectively (shown in Fig.5(b)5(c)).

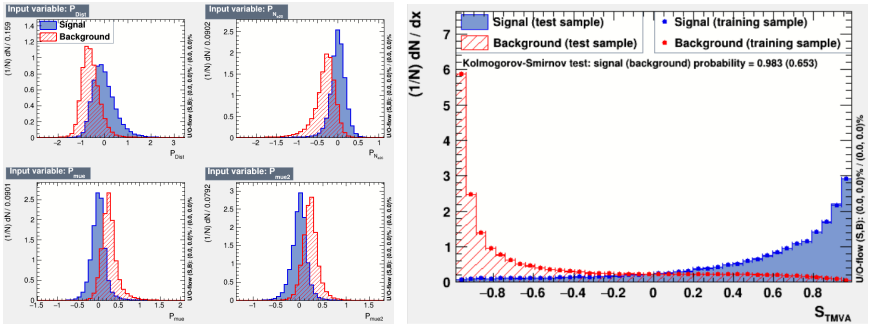

(a) (b)

Figure 4: (a) The distributions of P_{Dist}, $P_{N_{e20}}$, P_{mue} and P_{mue2}. Blue and red distribution represent protons and other heavier components, respectively. (b) Training result of BDTG classifier for protons.

4. Results

4.1 Proton spectrum in MC events

Once high-purity proton events are selected and the reconstructed energy distribution of the events is obtained, the cosmic ray proton energy spectrum can be obtained using the following formula:

$$\phi(E) = \frac{N(E) \times \epsilon(E)}{\Delta E \times T \times A_{eff} \times \eta(E)} \tag{2}$$

where $N(E)$ is the number of selected proton events. $\epsilon(E)$ is purity. T and A_{eff} are observation time and aperture, respectively. $\eta(E)$ is proton selection efficiency. In this work, half of the simulation events were randomly selected as experimental data to verify the feasibility of the analysis method.

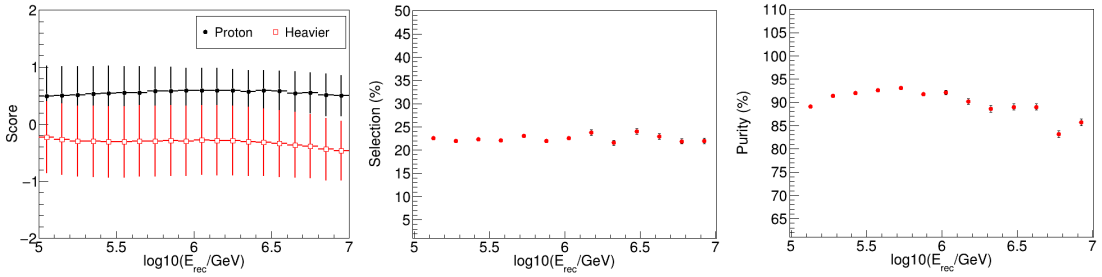

(a) (b) (c)

Figure 5: (a) Distribution of the S_{TMVA} as a function of reconstructed energy. The error bars show the RMS in each bin. Black filled circles and red open squares represent protons and heavier components, respectively. (b) and (c) is the selection efficiency and purity of proton events, respectively.

First, reassign the weight of the simulated events according to the Gaisser model [7]. Then, events were selected using the selection criteria in Sec.3.2. Finally, according to equation 2, the proton energy spectrum in the simulation is obtained (shown in Fig.6).

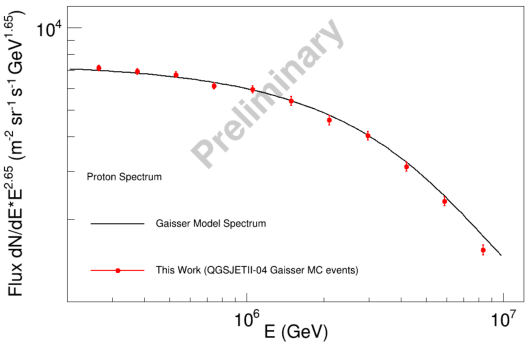

Figure 6: The proton spectrum in simulation based on the Gaisser model.

4.2 Systematic uncertainties

We randomly select half of the simulated events and assign them weights based on the Gaisser model [7] as experimental data. Comparing the proton energy spectra obtained under different conditions (reconstructed spectra) with the Gaisser model energy spectrum (model spectrum) is done to study the systematic uncertainties. The main sources of systematic uncertainties considered in this work are: (1) effects related to the assumed composition models used to determine selection efficiency and purity; (2) effects of different selection efficiency and purity due to the different proton selection conditions; (3) effects from different energy reconstruction methods; (4) effects from the hadronic interaction models used in the air-shower simulations.

Composition model: In this work, we use three composition model assumptions to study the systematic uncertainty: the Gaisser model, the Horandel model [8], and the equal quantity model. The equal quantity model means that the flux of five components is the same, and the energy spectrum index is -2.7. According to the three composition models, selecting proton events can yield three different selection efficiencies and purities. By applying these three selection efficiencies and purities to the simulated events, we obtained three reconstructed spectra of the Gaisser model

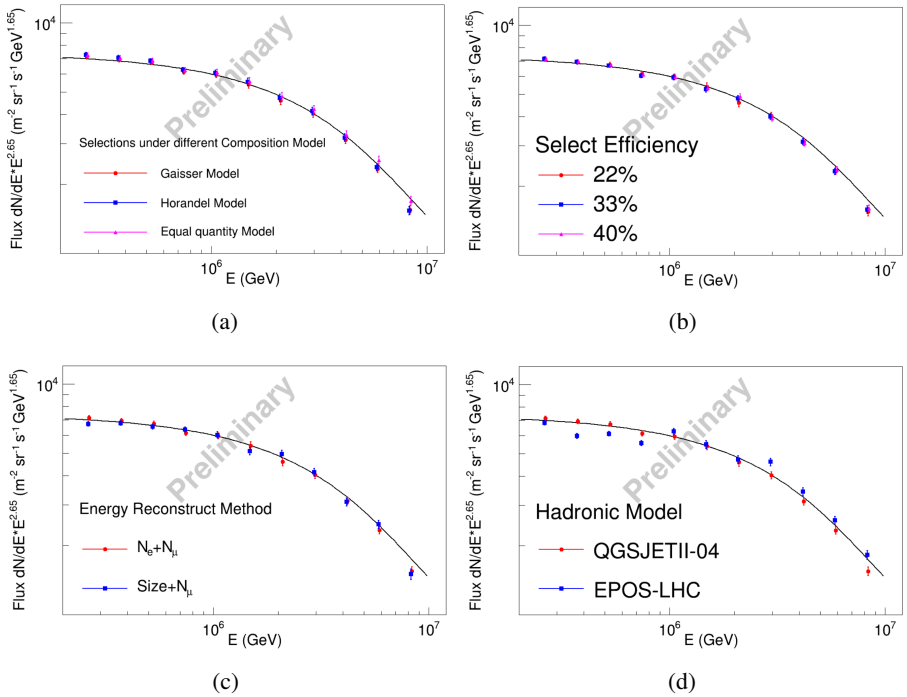

Figure 7: The solid lines in the four graphs represent the proton energy spectra based on the Gaisser model. The data points in the four graphs represent the proton energy spectra based on the Gaisser model obtained from simulation under different conditions. (a) Proton spectra based on the Gaisser model obtained under different event selections according to different composition models. (b) Proton spectra based on the Gaisser model were obtained under different selection efficiencies. (c) Proton spectra based on the Gaisser model obtained under different energy reconstruction methods. (d) Proton spectra based on the Gaisser model obtained under different hadronic interaction methods.

under different composition models. The differences between the reconstructed spectra and the model spectrum are less than 5% below 8 PeV. (shown in Fig.7(a)).

Selection conditions: The purity of proton events varies depending on the selection efficiency. We obtain proton spectra with different selection efficiency and purity by varying the selection conditions. The greater the difference between the spectral structure in the experiment and the model, the greater the difference in the final spectral results. The selection efficiency is 22%, 33%, and 44%, respectively, corresponding to 90%, 85% and 80% purity. The differences between the reconstructed spectra and the model spectrum are less than 5% below 8 PeV. (shown in Fig.7(b)).

Energy reconstruction method: Two energy reconstruction methods in Sec.3.1 yield two proton spectra. The differences between the reconstructed spectra and the model spectrum are less than 6% below 8 PeV. (shown in Fig.7(c))

Hadronic interaction models: To evaluate the influence of the uncertainties in the physics of the high energy hadronic interaction, we produced a small set of MC simulations using EPOS-LHC[9] and repeated the analysis procedure. The differences between the reconstructed spectra and the model spectrum are taken as systematic uncertainty from hadronic interaction models, which is less than 15% (shown in Fig.7(d)).

5. Summary

The Data set of hybrid observations with shower core inside the KM2A array has been obtained. These data contain 4×10^6 events with a corresponding observation time of 569 hours. Two energy reconstruction methods based on ED&MD and WFCTA&MD are studied in simulation. The resolution of energy reconstruction is less than 20% and 18% above 300 TeV for ED&MD and WFCTA&MD, respectively. Four composition identification parameters (P_{Dist} $P_{N_{e20}}$, P_{Dist} and $P_{N_{e20}}$) are combined in ROOT-TMVA to select proton events, and the purity of proton events is about 90%. Systematic uncertainties have also been studied. The largest systematic uncertainty comes from the hadronic interaction model, which is 15%. Experimental data will be used later to obtain the proton energy spectrum.

6. Acknowledgements

We would like to thank all staff members who work at the LHAASO site above 4400 meters above sea level year-round to maintain the detector and keep the water recycling system, electricity power supply and other components of the experiment operating smoothly. We are grateful to Chengdu Management Committee of Tianfu New Area for the constant financial support for research with LHAASO data. This research work is also supported by the following grants: The National Key R&D program of China under grants 2018YFA0404201, 2018YFA0404202, 2018YFA0404203, and 2018YFA0404204, by the National Natural Science Foundation of China, NSFC No.12022502, No.12205314, No. 12105301, No. 12261160362, No.12105294, No.U1931201, NSFC No. 12275280, No.11905240, No.12261141691, Innovation Project of IHEP No. E25451U2, Sichuan Province Science Foundation for Distinguished Young Scholars No.2022JDJQ0043, Sichuan Science and Technology Department No. 2023YFSY0014, Xiejialin Foundation of IHEP No.E2546IU2, and in Thailand by the NSRF via the Program Management Unit for Human Resources & Institutional Development, Research and Innovation (No. B37G660015).

References

[1] Benedetto D'Ettorre Piazzoli et al 2022 Chinese Phys. C 46 030004

[2] Heck D, Knapp J, Capdevielle J N, et al. 1998

[3] S. Ostapchenko, Phys. Rev. D 83 (2011) 014018.

[4] A. Ferrari et al., Report INFN/TC_05/11, SLAC-R-773, CERN-2005-10, 2005.

[5] H. Zhang, H. He, and C. Feng, Phys. Rev. D 106, 123028 (2022)

[6] L. Wang, L. Ma, S. Zhang, C. Feng, et al. Phys. Rev. D 107, 043036 (2023)

[7] Gaisser, T.K., Stanev, T. & Tilav, S. Front. Phys. 8, 748–758 (2013)

[8] HöRANDEL J R. Astroparticle Physics, 2003, 19(2):193–220

[9] T. Pierog et al., Phys. Rev. C 92 (2015) 034906.

Full Authors List: LHAASO Collaboration

Zhen Cao[1,2,3], F. Aharonian[4,5], Q. An[6,7], Axikegu[8], L.X. Bai[9], Y.X. Bai[1,3], L.X. Bai[9], Y.X. Bai[1,3], Y.W. Bao[10], D. Bastieri[11], X.J. Bi[1,2,3], Y.J. Bi[1,3], H. Cai[12], J.T. Cai[11], Zhe Cao[6,7], J. Chang[13], J.F. Chang[1,3,6], B.M. Chen[14], E.S. Chen[1,2,3], J. Chen[9], Liang Chen[1,2,3], Liang Chen[15], Long Chen[8], M.J. Chen[1,3], M.L. Chen[1,3,6], Q.H. Chen[8], S.H. Chen[1,2,3], S.Z. Chen[1,3], T.L. Chen[16],X.L. Chen[1,2,3], Y. Chen[10], N. Cheng[1,3], Y.D. Cheng[1,3], S.W. Cui[14], X.H. Cui[17], Y.D. Cui[18], B. D'Ettorre Piazzoli[19], B.Z. Dai[20], H.L. Dai[1,3,6], Z.G. Dai[7], Danzengluobu[16], D. della Volpe[21], X.J. Dong[1,3], K.K. Duan[13], J.H. Fan[11], Y.Z. Fan[13], Z.X. Fan[1,3], J. Fang[20], K. Fang[1,3], C.F. Feng[22], L. Feng[13], S.H. Feng[1,3], Y.L. Feng[13], B. Gao[1,3], C.D. Gao[22], L.Q. Gao[1,2,3], Q. Gao[16], W. Gao[22], M.M. Ge[20], L.S. Geng[1,3], G.H. Gong[23], Q.B. Gou[1,3], M.H. Gu[1,3,6], F.L. Guo[15], J.G. Guo[1,2,3], X.L. Guo[8], Y.Q. Guo[1,3], Y.Y. Guo[1,2,3,13], Y.A. Han[24], H.H. He[1,2,3], H.N. He[13], J.C. He[1,2,3], S.L. He[11], X.B. He[18], Y. He[8], M. Heller[21], Y.K. Hor[18], C. Hou[1,3], H.B. Hu[1,2,3], S. Hu[9], S.C. Hu[1,2,3], X.J. Hu[23], D.H. Huang[8], Q.L. Huang[1,3], W.H. Huang[22], X.T. Huang[22], X.Y. Huang[13], Z.C. Huang[8], F. Ji[1,3], X.L. Ji[1,3,6], H.Y. Jia[8], K. Jiang[6,7], Z.J. Jiang[20], C. Jin[1,2,3], T. Ke[1,3], D. Kuleshov[25], K. Levochkin[25], B.B. Li[14], Cheng Li[6,7], Cong Li[1,3], F. Li[1,3,6], H.B. Li[1,3], H.C. Li[1,3], H.Y. Li[7,13], J. Li[1,3,6], K. Li[1,3], W.L. Li[22], X.R. Li[1,3], Xin Li[6,7], Xin Li[8], Y. Li[9], Y.Z. Li[1,2,3], Zhe Li[1,3], Zhuo Li[26], E.W. Liang[27], Y.F. Liang[27], S.J. Lin[18], B. Liu[7], C. Liu[1,3], D. Liu[22], H. Liu[8], H.D. Liu[24], J. Liu[1,3], J.L. Liu[28], J.S. Liu[18], J.Y. Liu[1,3], M.Y. Liu[16], R.Y. Liu[10], S.M. Liu[8], W. Liu[1,3], Y. Liu[11], Y.N. Liu[23], Z.X. Liu[9], W.J. Long[8], R. Lu[20], H.K. Lv[1,3], B.Q. Ma[26], L.L. Ma[1,3], X.H. Ma[1,3], J.R. Mao[29], A. Masood[8], Z. Min[1,3], W. Mitthumsiri[30], T. Montaruli[21], Y.C. Nan[22], B.Y. Pang[8], P. Pattarakijwanich[30], Z.Y. Pei[11], M.Y. Qi[1,3], Y.Q. Qi[14], B.Q. Qiao[1,3], J.J. Qin[7], D. Ruffolo[30], V. Rulev[25], A. Sáiz[30], L. Shao[14], O. Shchegolev[25,31], X.D. Sheng[1,3], J.Y. Shi[1,3], H.C. Song[26], Yu.V. Stenkin[25,31], V. Stepanov[25], Y. Su[32], Q.N. Sun[8], X.N. Sun[27], Z.B. Sun[33], P.H.T. Tam[18], Z.B. Tang[6,7], W.W. Tian[2,17], B.D. Wang[1,3], C. Wang[33], H. Wang[8], H.G. Wang[11], J.C. Wang[29], J.S. Wang[28], L.P. Wang[22], L.Y. Wang[1,3], R.N. Wang[8], W. Wang[18], W. Wang[12], X.G. Wang[27], X.J. Wang[1,3], X.Y. Wang[10], Y. Wang[8], Y.D. Wang[1,3], Y.J. Wang[1,3], Y.P. Wang[1,2,3], Z.H. Wang[9], Z.X. Wang[20], Zhen Wang[28], Zheng Wang[1,3,6], D.M. Wei[13], J.J. Wei[13], Y.J. Wei[1,2,3], T. Wen[20], C.Y. Wu[1,3], H.R. Wu[1,3], S. Wu[1,3], W.X. Wu[8], X.F. Wu[13], S.Q. Xi[1,3], J. Xia[7,13], J.J. Xia[8], G.M. Xiang[2,15], D.X. Xiao[16], G. Xiao[1,3], H.B. Xiao[11], G.G. Xin[12], Y.L. Xin[8], Y. Xing[15], D.L. Xu[28], R.X. Xu[26], L. Xue[22], D.H. Yan[29], J.Z. Yan[13], C.W. Yang[9], F.F. Yang[1,3,6], J.Y. Yang[18], L.L. Yang[18], M.J. Yang[1,3], R.Z. Yang[7], S.B. Yang[20], Y.H. Yao[9], Z.G. Yao[1,3], Y.M. Ye[23], L.Q. Yin[1,3], N. Yin[22], X.H. You[1,3], Z.Y. You[1,2,3], Y.H. Yu[22], Q. Yuan[13], H.D. Zeng[13], T.X. Zeng[1,3,6], W. Zeng[20], Z.K. Zeng[1,2,3], M. Zha[1,3], X.X. Zhai[1,3], B.B. Zhang[10], H.M. Zhang[10], H.Y. Zhang[22], J.L. Zhang[17], J.W. Zhang[9], L.X. Zhang[11], Li Zhang[20], Lu Zhang[14], P.F. Zhang[20], P.P. Zhang[14], R. Zhang[7,13], S.R. Zhang[14], S.S. Zhang[1,3], X. Zhang[10], X.P. Zhang[1,3], Y.F. Zhang[8], Y.L. Zhang[1,3], Yi Zhang[1,13], Yong Zhang[1,3], B. Zhao[8], J. Zhao[1,3], L. Zhao[6,7], L.Z. Zhao[14], S.P. Zhao[13,22], F. Zheng[33], Y. Zheng[8], B. Zhou[1,3], H. Zhou[28], J.N. Zhou[15], P. Zhou[10], R. Zhou[9], X.X. Zhou[8], C.G. Zhu[22], F.R. Zhu[8], H. Zhu[17], K.J. Zhu[1,2,3,6] and X. Zuo[1,3]

[1]Key Laboratory of Particle Astrophyics & Experimental Physics Division & Computing Center, Institute of High Energy Physics, Chinese Academy of Sciences, 100049 Beijing, China.
[2]University of Chinese Academy of Sciences, 100049 Beijing, China.
[3]TIANFU Cosmic Ray Research Center, Chengdu, Sichuan, China.
[4]Dublin Institute for Advanced Studies, 31 Fitzwilliam Place, 2 Dublin, Ireland.
[5]Max-Planck-Institut for Nuclear Physics, P.O. Box 103980, 69029 Heidelberg, Germany.
[6]State Key Laboratory of Particle Detection and Electronics, China.
[7]University of Science and Technology of China, 230026 Hefei, Anhui, China.
[8]School of Physical Science and Technology & School of Information Science and Technology, Southwest Jiaotong University, 610031 Chengdu, Sichuan, China.
[9]College of Physics, Sichuan University, 610065 Chengdu, Sichuan, China.
[10]School of Astronomy and Space Science, Nanjing University, 210023 Nanjing, Jiangsu, China.
[11]Center for Astrophysics, Guangzhou University, 510006 Guangzhou, Guangdong, China.
[12]School of Physics and Technology, Wuhan University, 430072 Wuhan, Hubei, China.
[13]Key Laboratory of Dark Matter and Space Astronomy, Purple Mountain Observatory, Chinese Academy of Sciences, 210023 Nanjing, Jiangsu, China.
[14]Hebei Normal University, 050024 Shijiazhuang, Hebei, China.
[15]Key Laboratory for Research in Galaxies and Cosmology, Shanghai Astronomical Observatory, Chinese Academy of Sciences, 200030 Shanghai, China.
[16]Key Laboratory of Cosmic Rays (Tibet University), Ministry of Education, 850000 Lhasa, Tibet, China.
[17]National Astronomical Observatories, Chinese Academy of Sciences, 100101 Beijing, China.
[18]School of Physics and Astronomy & School of Physics (Guangzhou), Sun Yat-sen University, 519000 Zhuhai, Guangdong, China.
[19]Dipartimento di Fisica dell'Università di Napoli `Federico II", Complesso Universitario di Monte Sant'Angelo, via Cinthia, 80126 Napoli, Italy.
[20]School of Physics and Astronomy, Yunnan University, 650091 Kunming, Yunnan, China.
[21]Departement de Physique Nucleaire et Corpusculaire, Faculte de Sciences, Universite de Gen'eve, 24 Quai Ernest Ansermet, 1211 Geneva, Switzerland.
[22]Institute of Frontier and Interdisciplinary Science, Shandong University, 266237 Qingdao, Shandong, China.
[23]Department of Engineering Physics, Tsinghua University, 100084 Beijing, China.
[24]School of Physics and Microelectronics, Zhengzhou University, 450001 Zhengzhou, Henan, China.
[25]Institute for Nuclear Research of Russian Academy of Sciences, 117312 Moscow, Russia.

PoS(ICRC2023)423

[26]School of Physics, Peking University, 100871 Beijing, China.
[27]School of Physical Science and Technology, Guangxi University, 530004 Nanning, Guangxi, China.
[28]Tsung-Dao Lee Institute & School of Physics and Astronomy, Shanghai Jiao Tong University, 200240 Shanghai, China.
[29]Yunnan Observatories, Chinese Academy of Sciences, 650216 Kunming, Yunnan, China.
[30]Department of Physics, Faculty of Science, Mahidol University, 10400 Bangkok, Thailand.
[31]Moscow Institute of Physics and Technology, 141700 Moscow, Russia.
[32]Key Laboratory of Radio Astronomy, Purple Mountain Observatory, Chinese Academy of Sciences, 210023 Nanjing, Jiangsu, China.
[33]National Space Science Center, Chinese Academy of Sciences, 100190 Beijing, China.

PoS(ICRC2023)423